Metal Nanocrystals

DOI: 10.1002/anie.201100512

Oleylamine-Mediated Shape Evolution of Palladium Nanocrystals**

*Zhiqiang Niu, Qing Peng, Ming Gong, Hongpan Rong, and Yadong Li**

The properties of noble metal nanocrystals (NCs) are shape-related, especially for Au, Ag, Pd, and Pt.[1] Nonspherical Au and Ag NCs show distinct surface plasmon resonance,[2–4] and the catalytic activity of Pd and Pt NCs can be dictated by exposing different lattice planes and increasing the number of corners and edges.[5,6] Therefore, morphology control of noble metal NCs is critically important.

Various synthetic strategies have been developed to construct nonspherical noble metal NCs in hydrophilic solvents[7–17] such as water, ethylene glycol, and DMF. As a complement to the prevalent hydrophilic synthesis, shape control of noble metals in hydrophobic organic solvents is also necessary. Advantages of noble metal NCs made in hydrophobic solvents include narrow size distribution, tunable surface chemistry, and good compatibility with organic functional groups. First, monodisperse NCs[18–21] can easily self-assemble into highly ordered patterns, and thus facilitate fabrication of devices.[22] Moreover, monodispersity is of great importance for the study of size-related properties.[23] Second, in hydrophobic synthesis, the choice of surfactants is greatly expanded to carboxylic acids, alkane thiols, alkyl phosphines, alkyl amines, and so on, which will greatly enrich the surface chemistry of NCs and further influence their catalytic,[24] optical,[25] and magnetic properties.[26] For example, charge transport by Au and Ag NCs can be regulated by the length of alkane thiol molecules capping their surface.[27] Third, noble metal NCs can be modified with various functional organic groups in hydrophobic solvents to give advanced hybrid materials. For instance, by incorporating azobenzene groups in the ligands, hydrophobic Au NCs become capable of writing self-erasing images.[28]

Several groups have reported the synthesis of nonspherical hydrophobic noble metal NCs. Examples include Au nanowires obtained by reducing polymeric strands of Au^{+}–oleylamine (OAm) complex,[29,30] Pt nanocubes, multipods,[31–33] and Rh tetrahedra[34] prepared through gas-assisted (e.g., H_2, CO) synthesis, and Ag nanocubes obtained by oxidative etching.[35,36] Despite this success, systematic shape control of noble metal NCs in hydrophobic systems remains a challenging task, and the surfactant effects behind shape evolution need to be further identified. Herein we report an OAm-based system for synthesis of Pd NCs in toluene; icosa-, deca-, octa-, tetrahedral, and triangular platelike Pd NCs were systematically prepared. The synthesis follows a three-step "intermediates formation–nucleation–growth" process, during which OAm plays a key role in the shape evolution of Pd NCs by mediating the counterbalance between crystal strain and surface energy. The electrochemical activities of as-obtained Pd NCs were investigated in the oxidation of formic acid.

Palladium NCs were typically synthesized by stirring a mixture of OAm, formaldehyde, $[Pd(acac)_2]$ (acac = acetylacetonate), and toluene at room temperature in air, heating it in an autoclave at 100 °C for 8 h, and allowing it to slowly cool to ambient temperature (Scheme S1, Supporting Information). Figure 1 shows TEM images of the as-obtained Pd NCs. Generally, the products are all uniform and exclusively bound by well-defined {111} facets. Icosahedra have an edge length of 8.8 ± 0.6 nm. Their icosahedral shape can be identified by the hexagonal projections and the threefold twinned structure observed in Figure 1c. Decahedra have an edge length of 10.3 ± 0.8 nm. Their decahedral shape can be easily confirmed by the pentagonal profiles and fivefold twinned structure observed in Figure 1f. Octahedra with an edge length of 6.6 ± 0.5 nm can spontaneously assemble into large-scale 2D arrays on a copper grid (Figure 1g). Continuous lattice fringes in the high-resolution (HR) TEM image (Figure 1i) confirm its single-crystalline nature. When oriented along [001], [110], and [111], octahedra exhibited square, rhombic, and hexagonal projections, respectively (Figure S2, Supporting Information). Tetrahedra or truncated tetrahedra with an edge length of 12.9 ± 1.4 nm can also form patterned arrays on copper grid (Figure 1j). Although a triangular profile is observed in the TEM image, high-angle annular dark-field scanning TEM (HAADF-STEM) studies unveil their tetrahedral shape (Figure S3, Supporting Information). The triangular plates have an edge length of 17.3 ± 4.1 nm and a thickness of 6.6 ± 1.0 nm. Figure 1n shows a monolayer of patterned Pd triangular plates. We found that the as-obtained Pd triangular plates could form highly ordered 3D assemblies in two different ways by controlling their concentration (Figure S4, Supporting Information).

To elucidate the mechanism of this synthetic system, the roles of reagents were investigated in detail. First, we found OAm would coordinate to $[Pd(acac)_2]$ to form different intermediates under room temperature stirring. Figure 2a displays the evolution of UV/Vis spectra of a toluene solution containing $[Pd(acac)_2]$ and OAm. A strong adsorption peak around 329 nm was observed for pure $[Pd(acac)_2]$. After addition of 0.02 mL of OAm, the peak at 329 nm decreased while another adsorption peak at about 315 nm emerged, which can be attributed to the formation of $[Pd(acac)_x$-

[*] Z. Niu, Dr. Q. Peng, M. Gong, H. Rong, Prof. Y. Li
Department of Chemistry
Tsinghua University, Beijing, 100084 (P. R. China)
Fax: (+86) 10-6278-8765
E-mail: ydli@mail.tsinghua.edu.cn

[**] This work was supported by the State Key Project of Fundamental Research for Nanoscience and Nanotechnology (2011CB932401) and the Foundation for Innovative Research Groups of the National Natural Science Foundation of China (Grant No. 20921001).

Supporting information for this article is available on the WWW under http://dx.doi.org/10.1002/anie.201100512.

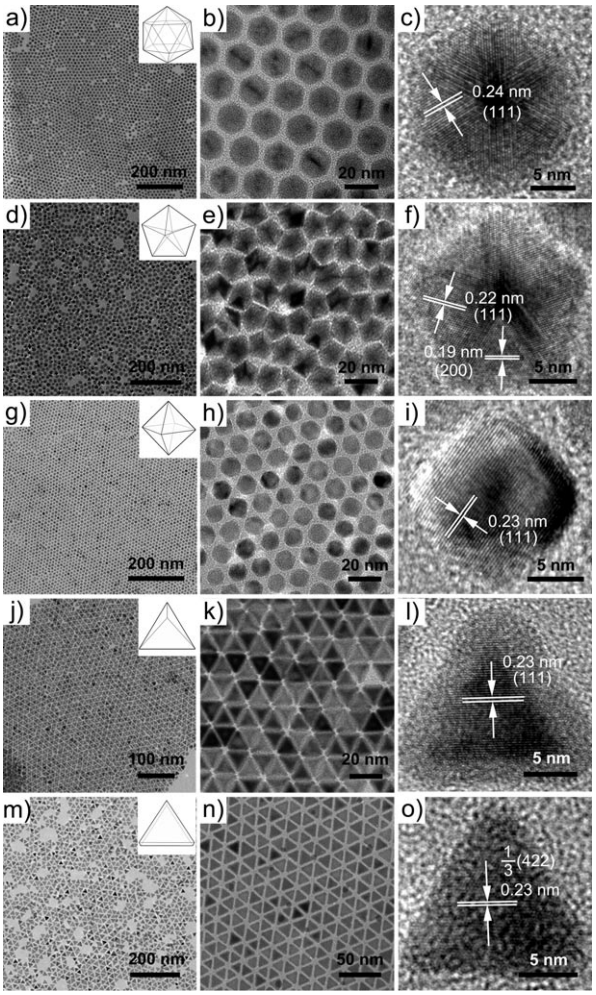

Figure 1. TEM images of Pd NCs with different shapes. a–c) icosahedron, d–f) decahedron, g–i) octahedron, j–l) tetrahedron, and m–o) triangular plate. Note that all of them can self-assemble into highly ordered patterns.

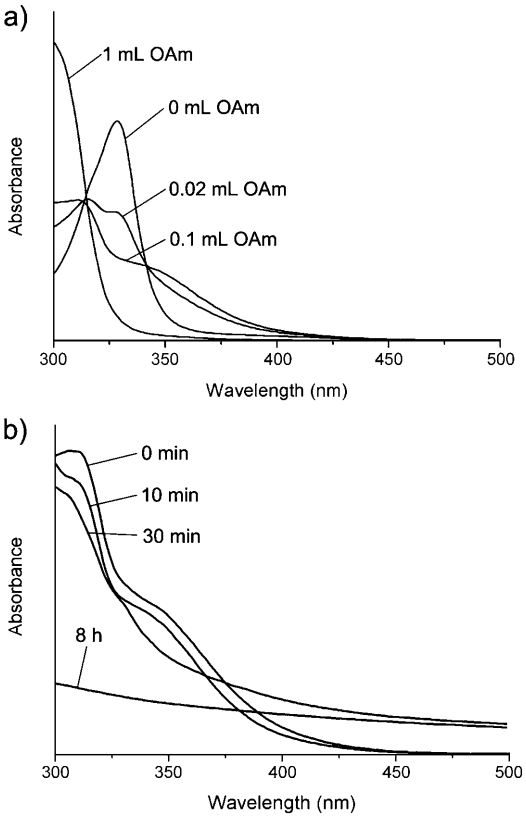

Figure 2. a) UV/Vis spectra of reaction solutions containing different amounts of OAm. b) Time-dependent UV/Vis spectra of the 0.1 mL OAm system after addition of formaldehyde: 0 and 10 min are at room temperature; 30 min and 8 h are under heating.

$(OAm)_y]$. When 0.1 mL of OAm was added, the adsorption peak at 329 nm further decreased and the peak at 315 nm underwent a slight blueshift to 311 nm indicating that more OAm coordinated to the Pd center. On increasing the quantity of OAm to 1 mL, the adsorption peak at 329 nm disappeared, which can be ascribed to complete release of acac ligands from the Pd center. Meanwhile, the whole plot developed into a strong adsorption edge corresponding to Pd–OAm complex. The observed spectral evolution indicates that different Pd intermediates, expressed as $[Pd(acac)_x(OAm)_y]$, can form by changing the dosage of OAm. These intermediates allow us to maneuver the reduction kinetics. For example, heating these intermediates at 100 °C in the presence of reductants for 2 min gave dark brown, brown, and colorless solutions for 0.02 mL, 0.1 mL, and 1 mL of OAm, respectively (Figure S5, Supporting Information). This result suggests that the reduction rates of Pd intermediates are decreased when more OAm coordinates to the Pd center.

We next investigated the role of formaldehyde. Formaldehyde first serves as a strong reducing agent which can even reduce $[Pd(acac)_2]$ at room temperature under overnight stirring. However, the final products produced in this way lack shape and size control to some extent (Supporting Information, Figure S6a). An improvement was made by stirring the reaction mixtures at room temperature to form nuclei and then heating them at elevated temperature to boost the growth. Taking the system with 0.1 mL of OAm as an example, we monitored the synthesis process by time-dependent UV/Vis spectroscopy (Figure 2b). Before addition of formaldehyde, the absorption curve shows the same profile of Pd intermediates as shown in Figure 2a. In the presence of formaldehyde, the color of the reaction solution remained yellow after stirring at room temperature for 10 min. However, the absorption peaks at 315 and 329 nm both decreased, that is, Pd intermediates were reduced to Pd nuclei or clusters. When the reaction proceeded under heating for 30 min, the yellow solution became dark brown. Correspondingly, the absorption peaks further decreased, and the whole plot was above the baseline due to scattering, which suggests that intermediates are continuously consumed for formation and growth of Pd NCs. The reaction solution became black after 8 h under heating, and the adsorption peaks at 315 and 329 nm had both vanished, that is, the intermediates were completely reduced to Pd NCs. Previous studies have shown that temporally discrete nucleation followed by growth on preformed nuclei is of critical importance for controlled synthesis of colloidal NCs,[37] and our synthesis coincides with

this strategy. To confirm the importance of a temporally discrete nucleation process, we heated the reaction mixture as soon as formaldehyde was added, and the final products were mixtures of polydisperse polygons (Figure S6b, Supporting Information).

Besides being a reducing agent, formaldehyde also acts as a selective capping agent to promote formation of {111} facets. The formaldehyde source used in our synthesis contains 12% methanol to limit formaldehyde oxidation and polymerization. To eliminate the effect of methanol, a control experiment under the same conditions but with complete replacement of formaldehyde by methanol was carried out. This resulted in 4.8 ± 1.6 nm elongated Pd nanoparticles without well-defined {111} facets (Figure S6c, Supporting Information). Replacing formaldehyde by benzaldehyde resulted in formation of 15.7 ± 3.1 nm multi-armed Pd nanostructures (Figure S6d, Supporting Information). This indicates that formaldehyde plays a unique role in selective formation of {111} facets in our synthesis.

Based on the above results, we propose a three-step "intermediates formation–nucleation–growth" mechanism (Scheme 1): different intermediates are formed by stirring the Pd precursor with OAm, addition of formaldehyde triggers the reduction of Pd intermediates to form crystal nuclei under room-temperature stirring, and these nuclei then aggregate into bigger nanoparticles at elevated temperature and further evolve into {111} faceted NCs with the aid of a surface capping agent (formaldehyde). While the intermediates formation allows us to manipulate the reduction kinetics of the synthesis, the temporal separation of nucleation and growth provides exquisite control over the final shapes of products.

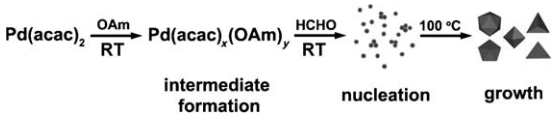

Scheme 1. Proposed mechanism for formation of Pd NCs.

To better understand the morphological evolution of Pd NCs, we employed a thermodynamic model for qualitative analysis (Scheme 2).[38] The total Gibbs free energies of Pd NCs are given by Equation (1), in which, U_c, U_s, U_e, and U_t are cohesive energy, surface energy, elastic strain energy, and twin-boundary energy respectively; V, S, and T are the volume, the total {111} surface area, and the twin-boundary area respectively; E_c, γ_{111}, W, and γ_t are the cohesive energy per unit volume, the {111} surface energy per unit area, the elastic strain energy density, and the twin-boundary energy per unit area respectively.

$$\begin{aligned} U &= U_c + U_s + U_e + U_t \\ &= V E_c + S \gamma_{111} + V W + T \gamma_t \end{aligned} \quad (1)$$

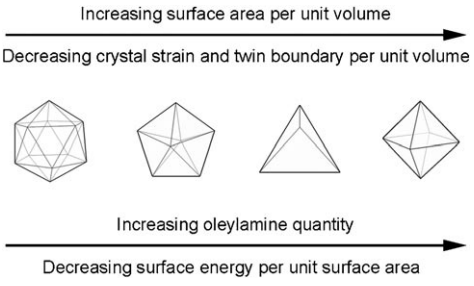

Scheme 2. Schematic illustration of shape evolution mediated by OAm.

In our experiments, the quantity of Pd precursors is the same, leading to Equation (2), in which the subscripts i, d, t, o, and p represent icosahedra, decahedra, tetrahedra, octahedra, and triangular plates respectively. Since E_c is constant, it can be concluded from Equations (1) and (2) that the cohesive energy U_c remains constant for systems with different amounts of OAm. Therefore, the morphological evolution of products mainly depends on the co-action of surface energy U_s, elastic strain energy U_e, and twin boundary energy U_t. Generally, the surface energy U_s can be tuned by means of the added quantity of surfactant (OAm), while elastic strain energy U_e and twin-boundary energy U_t are decided by the intrinsic structure of the NCs.

$$V_i = V_d + V_t = V_o + V_p \quad (2)$$

In the 0.02 mL OAm system, the surfaces of NCs lack sufficient protection because of low OAm concentration. Thus, this system has a high γ_{111} value and the U_s energy term plays a key role in determining the total free energy U. In this case, the product tends to adopt an icosahedral structure in an attempt to minimize its surface area. Other shapes, such as decahedron, octahedron, or tetrahedron, are prohibited due to their high surface-to-volume ratios (Table S1, Supporting Information).

In the 0.1 mL OAm system, the surfaces of NCs are well protected by surfactant. While the role of surface energy U_s is weaker, the effects of U_e and U_t can not be ignored. Icosahedra can be considered as an assembly of 20 single crystal tetrahedra. However, the inability of these tetrahedra to fully fill space gives rise to plenty of elastic strain and twin boundaries inside the icosahedron. Thus, to lower the total free energy U, the morphology of NCs evolved from icosahedron to decahedron and tetrahedron in the 0.1 mL OAm system. The decahedron is usually treated as an assembly of five single-crystal tetrahedra. The twin strain and boundary area inside a decahedron are much lower than in an icosahedron (Table S2, Supporting Information). At the same time, the surface-to-volume ratio of a decahedron is relatively low compared to octahedron, tetrahedron, and triangular plate. Therefore, formation of decahedra is a compromise between surface energy U_s and the energy terms due to twin structures (U_e and U_t). For the tetrahedron, due to its single-crystalline nature, its total free energy U is only decided by the surface energy U_s. With high surface-to-volume ratio, the formation of tetrahedron is prohibited in the high-γ_{111} system (0.02 mL OAm) but allowed when γ_{111} is decreased (0.1 mL OAm system).

In the 1 mL OAm system, the high concentration of OAm guarantees sufficient protection for NC surfaces. In this case, the role of surface energy U_s becomes subordinate and the energy terms U_e and U_t dominate. In other words, products with low elastic strain energy and low twin-boundary energy will be favored. Clearly, the strained decahedron will be disfavored in this system. Meanwhile, as shown in Table S1 of the Supporting Information, the surface-to-volume ratio of the tetrahedron is quite high. To further reduce the total Gibbs free energy, the products have a tendency to decrease their surface area. Consequently, the morphology of products evolved from decahedron and tetrahedron to octahedron.

Triangular plates are also obtained in the 1 mL OAm system. As demonstrated above, the reduction rate of [Pd(acac)$_2$] is the slowest in the 1 mL OAm system (Figure S4, Supporting Information). Previous studies in aqueous synthesis have indicated that Pd atoms tend to grow to platelike shapes though random hexagonal close packing when reduction is slow, in a kinetically controlled process.[8] In our case, formation of triangular plates is possible by the same mechanism.

The electrochemical catalytic properties of as-obtained Pd NCs were studied by the oxidation of formic acid. Figure 3 shows cyclic voltammograms of Pd NCs with different shapes. The peak potentials, peak current densities, and current densities at 0.3 V of the anodic scan are summarized in Table S3 of the Supporting Information. The maximum current densities in the oxidation of formic acid are in the order of icosahedra ≈ octahedra > tetrahedra > decahedra > triangular plates. Icosahedra, which expose the most corners, and octahedra, which have the smallest sizes, exhibited the highest oxidation rate of formic acid. A very sharp anodic peak at 0.49 V can be observed in the negative scan of octahedral Pd. This peak can be recognized as efficient reduction of Pd oxide film from the octahedral Pd surface.[39] Figure 3e shows the electrochemical performance of commercial Pd/C (Sigma-Aldrich 205699). The maximum current density was measured to be 0.70 mA cm^{-2} at 0.26 V, which is almost one seventh of that of Pd icosahedra.

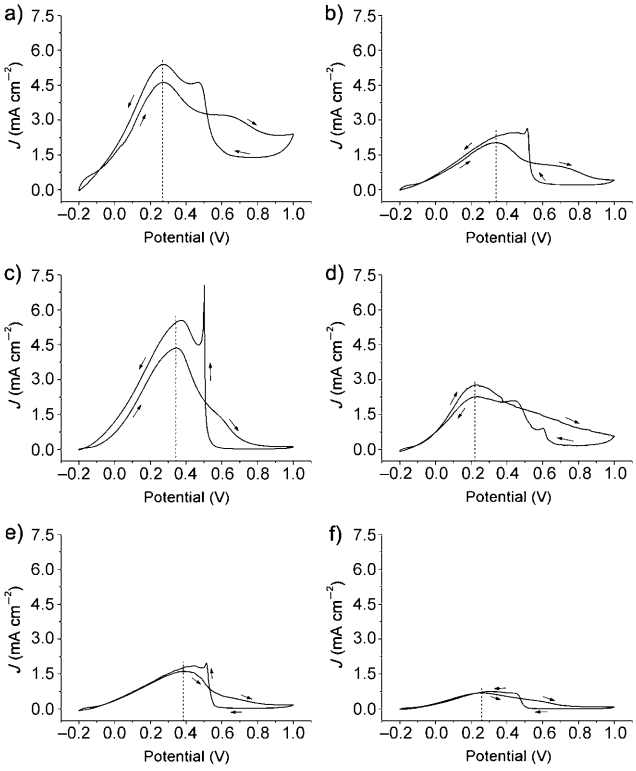

Figure 3. Cyclic voltammograms of Pd catalysts in 0.1 M $HClO_4$ and 2 M HCOOH solution at a scan rate of 50 mV s^{-1}. a) icosahedral Pd, b) decahedral Pd, c) octahedral Pd, d) tetrahedral Pd, e) triangular platelike Pd, and f) commercial Pd.

In summary, an OAm-based synthetic system was developed for the systematic shape control of Pd NCs. Icosa-, deca-, octa-, tetrahedral, and triangular platelike Pd NCs were selectively synthesized by varying the quantity of OAm. The formation process of these NCs was monitored by UV/Vis spectroscopy, which unveiled a three-step "intermediates formation–nucleation–growth" mechanism. The intermediates formation allows us to manipulate the reduction kinetics of the synthesis, and the temporal separation of nucleation and growth renders exquisite control over the final shapes of products. Thermodynamic model analysis suggests that OAm plays a crucial role in the shape evolution of Pd NCs. With increasing amount of OAm, the surface energy per unit area of NCs is dramatically reduced because more surfactant protects the surface. Therefore, multiple twinned particles (low surface-to-volume ratio, high strain) evolve into single-crystal particles (high surface-to-volume ratio, no strain). In addition, a catalytic study demonstrated high electrochemical activity of the as-obtained Pd NCs for the oxidation of formic acid.

Experimental Section

Synthesis of Pd NCs with different shapes: 12.2 mg of [Pd(acac)$_2$] and OAm were dissolved in 5 mL of toluene, and the solution was vigorously stirred for 10 min. 25 μL of formaldehyde was then added, and the mixture was stirred at room temperature for a further 10 min. The resulting solution was transferred to an autoclave and heated at 100 °C for 8 h and then slowly cooled to room temperature. The added quantities of OAm were as follows: 0.02 mL for icosahedra, 0.1 mL for decahedra and tetrahedra, and 1 mL for octahedra and triangular plates. For the synthesis of octahedra and triangular plates, the two 10 min stirring periods at room temperature were both reduced to 5 min. By cooling the products slowly, tetrahedra and triangular plates can be isolated from the growth solution by selective precipitation on the bottom the autoclave (Scheme S1, Supporting Information).

Characterization: X-ray diffraction patterns (Figure S1, Supporting Information) were recorded with a Rigaku D/max 2500Pc X-ray powder diffractometer with monochromatized $Cu_{K\alpha}$ radiation (λ = 1.5406 Å). TEM and HRTEM images were recorded by a JEOL JEM-1200EX working at 100 kV and a FEI Tecnai G2 F20 S-Twin working at 200 kV. The adsorption spectra were obtained with a Hitachi U-3010 UV/Vis spectrometer. Electrochemical measurements were conducted on CH Instrument 660D electrochemical analyzer.

Received: January 21, 2011
Revised: March 14, 2011
Published online: May 23, 2011

Keywords: crystal growth · electrochemistry · nanoparticles · palladium · solvothermal synthesis

[1] T. K. Sau, A. L. Rogach, F. Jackel, T. A. Klar, J. Feldmann, *Adv. Mater.* **2010**, *22*, 1805.
[2] A. Tao, P. Sinsermsuksakul, P. D. Yang, *Angew. Chem.* **2006**, *118*, 4713; *Angew. Chem. Int. Ed.* **2006**, *45*, 4597.
[3] B. J. Wiley, S. H. Im, Z. Y. Li, J. McLellan, A. Siekkinen, Y. Xia, *J. Phys. Chem. B* **2006**, *110*, 15666.
[4] L. Au, Y. C. Chen, F. Zhou, P. H. C. Camargo, B. Lim, Z. Y. Li, D. S. Ginger, Y. Xia, *Nano Res.* **2008**, *1*, 441.
[5] R. Narayanan, M. A. El-Sayed, *J. Phys. Chem. B* **2005**, *109*, 12663.
[6] K. M. Bratlie, H. Lee, K. Komvopoulos, P. D. Yang, G. A. Somorjai, *Nano Lett.* **2007**, *7*, 3097.
[7] A. R. Tao, S. Habas, P. D. Yang, *Small* **2008**, *4*, 310.
[8] Y. Xia, Y. J. Xiong, B. Lim, S. E. Skrabalak, *Angew. Chem.* **2009**, *121*, 62; *Angew. Chem. Int. Ed.* **2009**, *48*, 60.
[9] T. K. Sau, A. L. Rogach, *Adv. Mater.* **2010**, *22*, 1781.
[10] Y. G. Sun, Y. Xia, *Science* **2002**, *298*, 2176.
[11] C. C. Li, R. Sato, M. Kanehara, H. B. Zeng, Y. Bando, T. Teranishi, *Angew. Chem.* **2009**, *121*, 7015; *Angew. Chem. Int. Ed.* **2009**, *48*, 6883.
[12] B. Lim, M. J. Jiang, P. H. C. Camargo, E. C. Cho, J. Tao, X. M. Lu, Y. M. Zhu, Y. A. Xia, *Science* **2009**, *324*, 1302.
[13] W. X. Niu, L. Zhang, G. B. Xu, *ACS Nano* **2010**, *4*, 1987.
[14] Y. Y. Ma, J. Zeng, W. Y. Li, M. McKiernan, Z. X. Xie, Y. N. Xia, *Adv. Mater.* **2010**, *22*, 1930.
[15] X. Q. Huang, S. H. Tang, H. H. Zhang, Z. Y. Zhou, N. F. Zheng, *J. Am. Chem. Soc.* **2009**, *131*, 13916.
[16] X. Q. Huang, N. F. Zheng, *J. Am. Chem. Soc.* **2009**, *131*, 4602.
[17] N. Tian, Z. Y. Zhou, S. G. Sun, Y. Ding, Z. L. Wang, *Science* **2007**, *316*, 732.
[18] X. Wang, J. Zhuang, Q. Peng, Y. D. Li, *Nature* **2005**, *437*, 121.
[19] J. Park, J. Joo, S. G. Kwon, Y. Jang, T. Hyeon, *Angew. Chem.* **2007**, *119*, 4714; *Angew. Chem. Int. Ed.* **2007**, *46*, 4630.
[20] D. S. Wang, T. Xie, Q. Peng, Y. D. Li, *J. Am. Chem. Soc.* **2008**, *130*, 4016.
[21] W. Chen, R. Yu, L. L. Li, A. N. Wang, Q. Peng, Y. D. Li, *Angew. Chem.* **2010**, *122*, 2979; *Angew. Chem. Int. Ed.* **2010**, *49*, 2917.
[22] D. V. Talapin, J. S. Lee, M. V. Kovalenko, E. V. Shevchenko, *Chem. Rev.* **2010**, *110*, 389.
[23] S. Link, M. A. El-Sayed, *J. Phys. Chem. B* **1999**, *103*, 4212.
[24] H. Lee, S. E. Habas, S. Kweskin, D. Butcher, G. A. Somorjai, P. D. Yang, *Angew. Chem.* **2006**, *118*, 7988; *Angew. Chem. Int. Ed.* **2006**, *45*, 7824.
[25] M. Kuno, J. K. Lee, B. O. Dabbousi, F. V. Mikulec, M. G. Bawendi, *J. Chem. Phys.* **1997**, *106*, 9869.
[26] C. B. Murray, S. H. Sun, H. Doyle, T. Betley, *MRS Bull.* **2001**, *26*, 985.
[27] A. Zabet-Khosousi, A. A. Dhirani, *Chem. Rev.* **2008**, *108*, 4072.
[28] R. Klajn, P. J. Wesson, K. J. M. Bishop, B. A. Grzybowski, *Angew. Chem.* **2009**, *121*, 7169; *Angew. Chem. Int. Ed.* **2009**, *48*, 7035.
[29] Z. Y. Huo, C. K. Tsung, W. Y. Huang, X. F. Zhang, P. D. Yang, *Nano Lett.* **2008**, *8*, 2041.
[30] X. M. Lu, M. S. Yavuz, H. Y. Tuan, B. A. Korgel, Y. N. Xia, *J. Am. Chem. Soc.* **2008**, *130*, 8900.
[31] J. Ren, R. D. Tilley, *Small* **2007**, *3*, 1508.
[32] Y. J. Kang, X. C. Ye, C. B. Murray, *Angew. Chem.* **2010**, *122*, 6292; *Angew. Chem. Int. Ed.* **2010**, *49*, 6156.
[33] S. I. Lim, I. Ojea-Jimenez, M. Varon, E. Casals, J. Arbiol, V. Puntes, *Nano Lett.* **2010**, *10*, 964.
[34] K. H. Park, K. Jang, H. J. Kim, S. U. Son, *Angew. Chem.* **2007**, *119*, 1857; *Angew. Chem. Int. Ed.* **2007**, *46*, 1152.
[35] Y. Y. Ma, W. Y. Li, J. Zeng, M. McKiernan, Z. X. Xie, Y. N. Xia, *J. Mater. Chem.* **2010**, *20*, 3586.
[36] S. Peng, Y. Sun, *Chem. Mater.* **2010**, *22*, 6272.
[37] C. B. Murray, D. J. Norris, M. G. Bawendi, *J. Am. Chem. Soc.* **1993**, *115*, 8706.
[38] T. Ling, J. Zhu, H. M. Yu, L. Xie, *J. Phys. Chem. C* **2009**, *113*, 9450.
[39] M. I. Manzanares, A. G. Pavese, V. M. Solis, *J. Electroanal. Chem.* **1991**, *310*, 159.

